Original Article

Establishment of an orthotopic model of lung cancer by transthoracic lung puncture using tumor fragments

Wei Gan[1], Yi-Ming He[1], Fang-Ling Hu[2], Bin Xu[1], Yun-Kun Liu[1], An-Ji Wang[3], Yuan-Qiao He[4,5], Guo-Wen Zou[1]^

[1]Department of Thoracic Surgery, The First Affiliated Hospital, Nanchang University, Nanchang, China; [2]Department of Otolaryngology-Head and Neck Surgery, The First Affiliated Hospital, Nanchang University, Nanchang, China; [3]Medical College of Nanchang University, Nanchang, China; [4]Department of Laboratory Animal Science, Nanchang University, Nanchang, China; [5]Nanchang Royo Biotech Ltd., Nanchang, China

Contributions: (I) Conception and design: YQ He, GW Zou; (II) Administrative support: None; (III) Provision of study materials or patients: None; (IV) Collection and assembly of data: None; (V) Data analysis and interpretation: None; (VI) Manuscript writing: All authors; (VII) Final approval of manuscript: All authors.

Correspondence to: Guo-Wen Zou. Department of Thoracic Surgery, The First Affiliated Hospital, Nanchang University, Nanchang 330006, China. Email: guowenzou1988@163.com; Yuan-Qiao He. Department of Laboratory Animal Science, Nanchang University, Nanchang, China; Nanchang Royo Biotech Ltd., Nanchang, China. Email: heyuanqiao@ncu.edu.cn.

Background: Orthotopic models of lung cancer have been widely utilized, and the purpose of this study was to demonstrate the viability of our proposed modified modeling approach.

Methods: A total of 50 female BALB/c mice were implanted with 1×1×1 mm fragments of a tumor sample into the left lung lobe. After 2 months of observation, the mice were humanely euthanized through CO_2 inhalation. The macroscopic specimens were photographed, and the most representative neoplastic lesions were collected for histological analysis. Small-animal positron emission tomography/computed tomography (PET/CT) scans were conducted on 6 randomly selected mice.

Results: Local tumor formation, ipsilateral thoracic tissue infiltration, the contralateral chest wall, right lung metastases, and distant kidney metastases were observed in these models. Overall, the tumor development and metastasis rates were 60.86% (28/46) and 57.14% (16/28), respectively. The 3 mice that had a small-animal PET/CT scan developed a local tumor, but no distant metastases were observed.

Conclusions: This modified method was deemed reliable, reproducible, minimally invasive, straightforward, and comprehensible; it might serve as the foundation for developing patient-derived orthotopic xenografts of lung cancer.

Keywords: Lung cancer; orthotopic model; lung puncture; tumor fragments

Introduction

The significance of a xenograft model for lung cancer research is obvious, not only for understanding basic tumor biology but also for the development and validation of new tumor intervention strategies (1). Which could be classified into two broad groups according to the location of tumor inoculation—orthotopic and ectopic tumor model (2). The subcutaneous tumor xenograft is the most popular model but it remains controversial as these models rarely metastasize and can't represent the biological characteristics

^ ORCID: 0000-0001-8088-1458.

of lung cancer *in vivo*. Orthotopic tumor models, however, simulate the human pathophysiologic condition including tumor expansion, vascularization, and invasion as well metastasis. It is more representative to use an orthotopic lung cancer model to explore the mechanism of tumor progression (3).

Several approaches for creating orthotopic lung cancer models have been described in previous studies, including cell suspension transthoracic injection (4-6), intrabronchial injection (7), and orthotopic surgical implantation (8). Subsequently, Hoffman developed a patient-derived orthotopic xenograft (PDOX) nude mice model using orthotopic surgical implantation (9). A study showed that the amount of metastasis in orthotopic animals with implanted intact tumor tissue was larger than in orthotopic mice with implanted cell suspensions (10). In the late 1980s and early 1990s, orthotopic models experienced a modicum of popularity, but eventually, they faded into oblivion (9). Recent research on anticancer medications has transitioned from cytotoxic drugs targeting all molecules to those targeting specific molecules (11). Particularly, the introduction of the precision medicine project offers a tremendous opportunity for the creation and deployment of animal models, such as patient-derived xenograft (PDX) and PDOX (12).

Remarkably, orthotopic surgical implantation is the

primary technique for establishing a PDOX. However, this surgery requires a thoracotomy, a surgical suture to fix intact lung tissue, and general anesthesia. In preclinical studies of lung cancer patients, techniques that are intricate, technically challenging, and inflict severe trauma to mice have not been routinely utilized (13,14). Previously, we proposed the novel concept that PDOX may be generated through transthoracic lung puncture utilizing lung cancer tissue fragments harvested from the patient. However, this technique entails substantial difficulties in collecting clinical tumor samples, expense of immunodeficient mice, longer time of tumorigenesis, and a lower tumorigenesis rate. Therefore, we used Lewis lung cancer (LLC) and BALB/c mice to construct an orthotopic lung cancer practice model. The objective of this study was to demonstrate the feasibility of the modified method. We present the following article in accordance with the ARRIVE reporting checklist (available at https://jtd.amegroups.com/article/view/10.21037/jtd-23-439/rc).

Methods

Study design

This observational study was designed to demonstrate the viability of the modified modeling approach we proposed. A protocol was prepared before the study without registration. Firstly, we used LLC cells to construct subcutaneous models to provide tumor fragments for orthotopic models. The tumor fragments were then transplanted to the left lung lobe of mice (N=50) through lung puncture, followed by postoperative observation for 2 months. We randomly selected 4 mice from the group for sacrifice at weeks 2, 3, 4, 5, 6, and 7 following orthotopic implantation to assess local tumor progression. To better monitor the progression and metastasis of LLC after implantation, small-animal positron emission tomography/computed tomography (PET/CT) scans were performed on 6 mice. All gross specimens were photographed to better analyze the tumor's features, and the most representative neoplastic lesions in the left lung were collected for histological analysis.

Cell culture

LLC cells provided by China Center For Type Culture Collection (CCTCC; Hubei, China) were grown in Roswell Park Memorial Institute (RPMI) medium with 10% fetal bovine serum (FBS; TBD Science Biotechnology,


Highlight box

Key findings
- This modified method for establishing an orthotopic model of lung cancer was deemed reliable, reproducible, minimally invasive, and comprehensible.

What is known and what is new?
- Several approaches for creating orthotopic lung cancer models have been described in previous studies, including cell suspension transthoracic injection, intrabronchial injection, and orthotopic surgical implantation.
- Based on the work of the predecessors, we proposed to establish an orthotopic model of lung cancer through transthoracic lung puncture utilizing lung cancer tissue fragments. The purpose of this study was to demonstrate the viability of the modified modeling approach.

What is the implication, and what should change now?
- This modified method is reliable and reproducible, and can be mastered by beginners through simple practice. More importantly, it might serve as the foundation for developing patient-derived orthotopic xenografts of lung cancer.
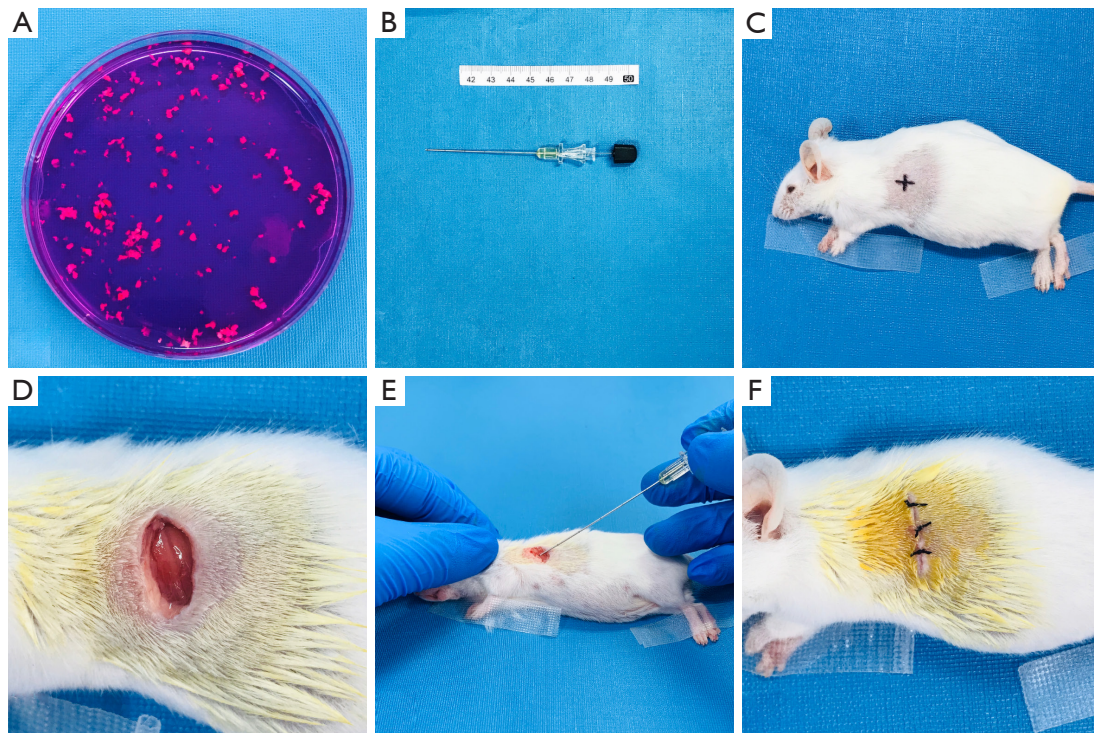
Figure 1 Procedures of establishing orthotopic lung cancer models. (A) A tumor harvested from a single mouse was cut into small pieces (1×1×1 mm). (B) An 18-gauge TEMNO soft tissue aspiration needle. (C) Animals were anesthetized and shaved off the hair around the operational location. The intersection between the midaxillary line and the 8th or 9th intercostal space was selected as the puncture point. (D) A skin incision was made on the left chest wall, and chest muscles were separated. (E) The needle with the prepared tissue block was inserted into the lung through the intercostal muscle approximately 6–9 mm, pushed the tissue out, and pulled the needle out slowly five seconds later. (F) Closed the skin and chest muscle with a 6-0 surgical suture.

Tianjin, China), L-glutamine, and gentamicin (Gibco BRL, Gaithersburg, MD, USA) at humidified 37 ℃/5% CO_2 incubators at either 2% or ambient O_2 for 1–2 days. Cells of the logarithmic phase were trypsinized, centrifuged, and suspended in RPMI-1640 medium. The cells were pelleted at a concentration of 5×10^6/mL for subcutaneous implantation.

Mouse

Female BALB/c mice aged 6–8 weeks were procured from Beijing Vital River Laboratory Animal Technology Ltd. (Beijing, China) and cared for according to the institution's animal care procedures. Under pathogen-free conditions, mice were fed a commercial mouse diet in a 12-hour light-dark cycle. The Institutional Animal Care and Use Committee of Nanchang Royo Biotech Ltd. (Nanchang, China) sanctioned all animal experiments (IACUC Issue

No. RYE2020021801). Animal experiments were performed in Nanchang Royo Biotech Ltd. (Nanchang, China), in compliance with institutional guidelines for the care and use of animals.

Orthotopic lung cancer model

LLC cells (5×10^6) suspended in 200 µL RPMI 1640 medium without FBS were injected subcutaneously into the right front flanks of BALB/c mice. As the subcutaneous tumor developed to approximately 1,000–1,500 mm³, a tumor harvested from a single mouse was cut into small pieces (1×1×1 mm) and implanted into the left lobe of the lung in additional mice (*Figure 1*). Each step is described in detail in the following sections. First, animals were sedated with an intraperitoneal injection of 50 mg/kg pentobarbital sodium, and then they were placed in a right lateral decubitus position with all 4 limbs secured. The area surrounding the

operative location was shaved. As the puncture location, the intersection between the midaxillary line and the 8th or 9th intercostal gap was chosen (*Figure 1C*). After iodophor disinfection, a 0.8–1.0 cm transverse skin incision was performed in the left chest wall approximately 2–4 mm from the costal arch. Sharp dissection separated the chest muscles, revealing the intercostal muscles and the left lung (*Figure 1D*). An 18-gauge TEMNO soft tissue aspiration needle (Merit Medical, South Jordan, UT, USA) was inserted into the lung through the intercostal muscle around 6–9 mm (the precise insertion depth was dependent on the size of the mice), along the long axis of the lung, and at an angle of 30 degrees to the horizontal (*Figure 1B,1E*). The prepared tissue block was then pushed out of the trocar needle gently and smoothly, the needle was rotated once slowly and was withdrawn 5 seconds later. After that, the skin and chest muscles were closed with a single layer of 6-0 surgical suture (*Figure 1F*). In an incubator at 37 ℃, anesthesia resuscitation was administered after surgery.

Small-animal PET/CT

As previously reported, all scans were performed on a small animal PET/CT (MIRA) scanner [PINGSENG Healthcare (Kunshan) Inc., Kunshan, China] (15). The mice for PET/CT tests fasted for 24 hours while having access to water. The mice were subsequently placed in the prone position on the PET/CT scanner bed, and scans were collected in the craniocaudal direction. The mice were weighed, sedated using isoflurane inhalation, and injected with 260 ci of ^{18}F-fluorodeoxyglucose (^{18}F-FDG) through a catheter placed in the tail vein. First, a CT scan was performed with a voltage of 80 kV and a current of 0.6 mA, using the Feldkamp (FDK) algorithm. After mice had metabolized the medication for 1 hour, a 10-minute PET scan was performed to collect data. The transaxial field of view (TFOV) was set to 60 mm, the axial field of view (AFOV) was set to 130 mm, and the 3-dimensional (3D) ordered subset expectation maximization (3D-OSEM) algorithm was utilized. The manufacturer's software (Avatar1.5.2; PINGSENG Healthcare (Kunshan) Inc. China) automatically merged PET and CT pictures.

Histopathological evaluation

The histopathological evaluation was performed as previously described (16). Briefly, BALB/c mice were sacrificed through CO_2 inhalation, and major organs (bilateral lungs, heart, liver, kidneys, adrenal glands, and mediastinal tissues) were removed, fixed in 10% formalin, and embedded in paraffin. The specimens were subsequently sectioned with a microtome to yield 4–5 mm-thick paraffin sections. Paraffin sections stained with hematoxylin and eosin (H&E) were examined under a light microscope.

Outcomes

The primary experimental outcomes were local tumor growth and metastasis rates. And the secondary outcome was the short-term perioperative outcome for constructing the orthotopic models.

Statistical analysis

Statistical analysis was performed using SPSS 23.0 (IBM Corp., Armonk, NY, USA). Descriptive analysis was presented as the mean ± standard deviation for continuous variables and frequency with percentages for categorical variables.

Results

Establishment of LLC orthotopic models

A specimen from a subcutaneous tumor was cut into 1×1×1 mm fragments and engrafted into the left lung lobe of 50 mice using the technique mentioned above. The entire process took around 6 minutes for each mouse. There were 2 mice that died during anesthesia resuscitation following the operation, and 2 died the next day. Autopsy revealed that all dead mice developed hemothorax of varying degrees after implantation. This leads to the development of atelectasis and respiratory failure, so we speculate that pulmonary hemorrhage and pulmonary atelectasis accounted for the majority of the 72-hour surgical mortality, which was less than 10%. The remaining mice were monitored for 2 months daily. They were humanely euthanized by CO_2 inhalation when they were moribund due to respiratory failure brought on by a heavy tumor load, prostration, and severe lung infections. *Table 1* displays the incidence of tumor growth and metastasis in BALB/c mice following transplantation. Overall, the tumor development and metastasis rates were 60.86% (28/46) and 57.14% (16/28), respectively.

2016

Gan et al. Establishment of the orthotopic model of lung cancer

Table 1 Growth characteristics of orthotopic models of lung cancer

Lewis lung cancer	BALB/c mice
Overall observation	46
Tumor incidence[#]	28
Tumor metastasis*	16
Mediastinum	15
Right lung	5
Chest wall	12
Diaphragm	6
Distant metastasis	1

Tumor incidence[#] and number of mice with metastasis* included the euthanatized mice.

Table 2 Orthotopic tumor growth and metastasis of Lewis lung cancer tissue in BALB/c mice

Condition	2 weeks	3 weeks	4 weeks	5 weeks	6 weeks	7 weeks
Local tumor growth	1/4	4/4	3/4	1/4	1/4	2/4
Metastasis	0/4	2/4	2/4	1/4	1/4	1/4

Local tumor growth

To assess local tumor progression, 4 mice were randomly selected from the group and sacrificed at weeks 2, 3, 4, 5, 6, and 7 following orthotopic implantation. *Table 2* shows the incidence of tumor growth and metastasis in BALB/c mice. In this model, the site of tumor formation was restricted to the left lung, and the size of the local tumors grew gradually; nevertheless, the number of tumors at the puncture site remained nearly constant regardless of time (*Figure 2A-2C*). During the initial stages, the tumor was typically stiff and white, and translucent in hue (*Figure 2D*). As the tumor grew, it got softer and paler, and some of the tumors developed necrosis and ulcers. A portion of the mice died of respiratory failure due to the tumor's expansion and pulmonary congestion (*Figure 2E,2F*). Histopathological examination confirmed the diagnosis of every tumor nodule.

Metastasis after orthotopic implantation

Tumor formation in the lungs of mice was not observed until day 10. As the size of the local tumor grew, it spread to the ipsilateral pulmonary pleura, chest wall, mediastinal and hilar lymph nodes, and then to the mediastinum and diaphragm (*Figure 3A-3C*). On days 35 and 42, tumor metastases were observed on the right chest wall and right lung, respectively (*Figure 3D,3E*). Moreover, in a 49-day-old model, it was observed that the tumor had spread to the kidney (*Figure 3F*). With time, the frequency of metastasis to the mediastinum and left chest wall increased relative to the contralateral chest and lungs. In addition, only 1 distant metastasis was discovered in 16 models with metastasis (*Table 1*). Pathological testing indicated that the heterogeneity of both metastatic and local tumors was consistent.

Implanted tumors could be revealed by small-animal PET/CT

To better monitor the progression and metastasis of LLC after implantation, small-animal PET/CT scans were performed on 6 mice; 3/6 exhibited local tumor formation, but no distant metastases were detected. Combining CT and PET scans defined tumors in mice strain BALB/c. Intense FDG uptake was demonstrated in the left lung tumor; it can be detected and measured in the transverse section, sagittal plane, and coronal plane, and the 3D reconstruction provides a clearer picture (*Figure 4*).

Histopathologic examination of implanted tumors in BALB/c mice

All *in vitro* observed local tumors and metastases were confirmed by pathological investigation of mice. Photographs of representative H&E-stained tumor slices depict the sequential course of tumor growth. At 14 days after implantation, we observed the development of solitary tiny nodules surrounded by hemocytes, inflammatory cells, and normal lung tissue (*Figure 5A*). Initially, the boundary between the tumor and adjacent tissue was distinct. However, as the tumor spread, it became blurry and eventually disappeared. In normal lung tissue, we noticed tumor cells with large hyperchromatic patchy nuclei and numerous mitotic fibers. Central portions of big tumor masses exhibited necrotic regions (*Figure 5B*). The heterogeneity and morphology of the mediastinal lymph nodes, chest wall, and contralateral lung metastases were consistent with those of the primary malignancies (*Figure 5C-5H*). Both kept their LLC morphology to a significant degree. Moreover, renal metastases were identified (*Figure 5I*). Consequently, these findings may indicate that the model has spontaneous distant metastases.

Figure 2 Representative local tumor growth in the left lung. (A-D) The site of tumor formation was confined to the left lung, and the size of the local tumors enlarged gradually (A, 14 days after implantation; B, 21 days after implantation; C, 28 days after implantation; D, 35 days after implantation). (E,F) As the enlargement of the tumor, it became soft and pale and some of the tumors appeared with necrosis and ulcer changes (E, 42 days after implantation and F, 49 days after implantation). The area indicated by the black arrows are the tumor lesion.

Discussion

In this study, we established orthotopic lung cancer models in BALB/c mice through transthoracic lung puncture using LLC tumor fragments. All gross specimens were photographed to better analyze the tumor's features, and the most representative neoplastic lesions in the left lung were collected for histological analysis. Local tumor formation, ipsilateral thoracic tissue infiltration, contralateral chest wall, right lung metastases, and distant kidney metastases were observed in these models. These processes resembled the biological patterns of primary tumor development, progression, and spontaneous metastasis (9,17). Pathological analysis indicated that the histological characteristics of the metastatic tumor were identical to those of the initial tumor. In addition, we utilized PET/CT on small animals to monitor tumor growth. During non-invasive image analysis, the specialized PET scanner for small animals displayed images with a high level of detail, allowing the structural properties of the tumor and the tight interaction of surrounding tissues to be demonstrated. Our results

demonstrated that this modified method we proposed was safe, feasible, and has great application prospects.

Paget suggested the 'seed and soil' hypothesis to explain the non-random pattern of tumor spread a century ago (18). With the validation and expansion of this concept, a greater understanding of the tumor microenvironment was achieved (17). The biological heterogeneity of cancer cells in the primary tumor and metastasis is the biggest impediment to metastasis treatment (19). In addition, the organ-specific microenvironment can alter the responsiveness of metastatic tumor cells to systemic therapy (20). In many cases, preclinical investigations indicate a positive response to newly produced medications, whereas clinical application reveals weak or even nonexistent therapeutic effects. Drug resistance and tumor metastasis are global issues that require more fundamental research for further investigation. As a result of poor translational research, it is also sometimes required to innovate or enhance modeling techniques (21). A recent study has demonstrated that organ-site-specific implantation of tumor cells is crucial for
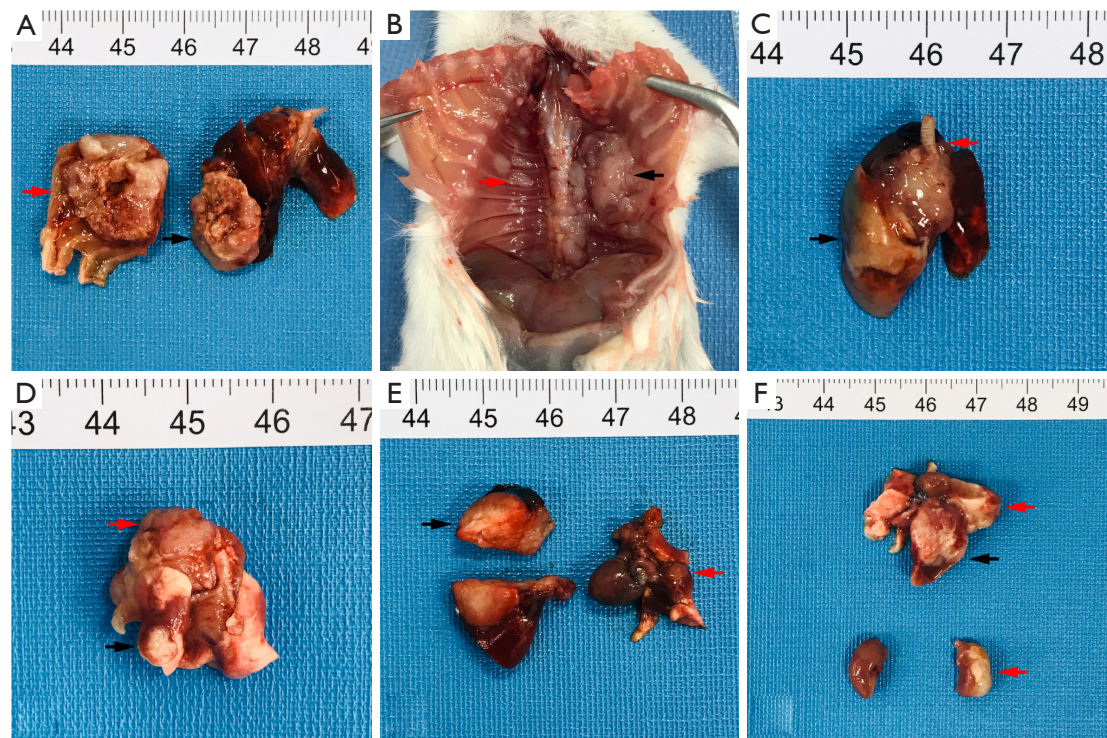
Figure 3 Typical tumor metastasis after orthotopic implantation. (A-C) The tumor invaded the ipsilateral pulmonary pleura, chest wall, and mediastinal and hilar lymph nodes and subsequently disseminated to the mediastinum and diaphragm. (D,E) The tumor metastasized to the right chest wall and right lung until day 35 and 42, respectively. (F) On day 49 after implantation, the tumor involved the thymus and distant metastasized to the kidney. The black arrows represent primary tumors and the red arrows represent metastatic tumors.
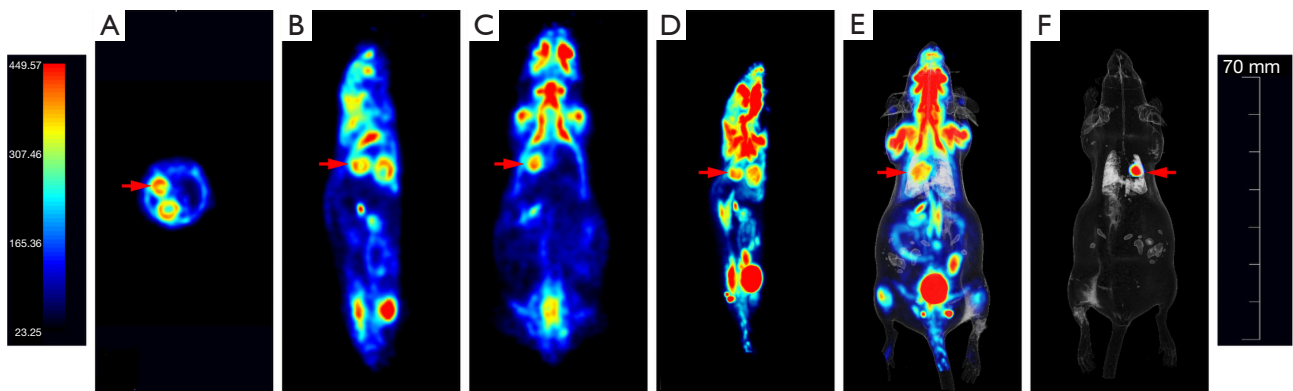
Figure 4 Small-animal PET/CT imaging of orthotopic lung cancer model. (A-C) Transverse section, sagittal plane, and coronal plane images. (D) PET three-dimensional reconstruction image. (E,F) PET/CT 3-dimensional reconstruction images image. FDG was specifically accumulated in the tumor and the heart in the thoracic cavity; the position and condition of the tumor could be determined clearly (red arrows). PET/CT, positron emission tomography/computed tomography; FDG, fluorodeoxyglucose.
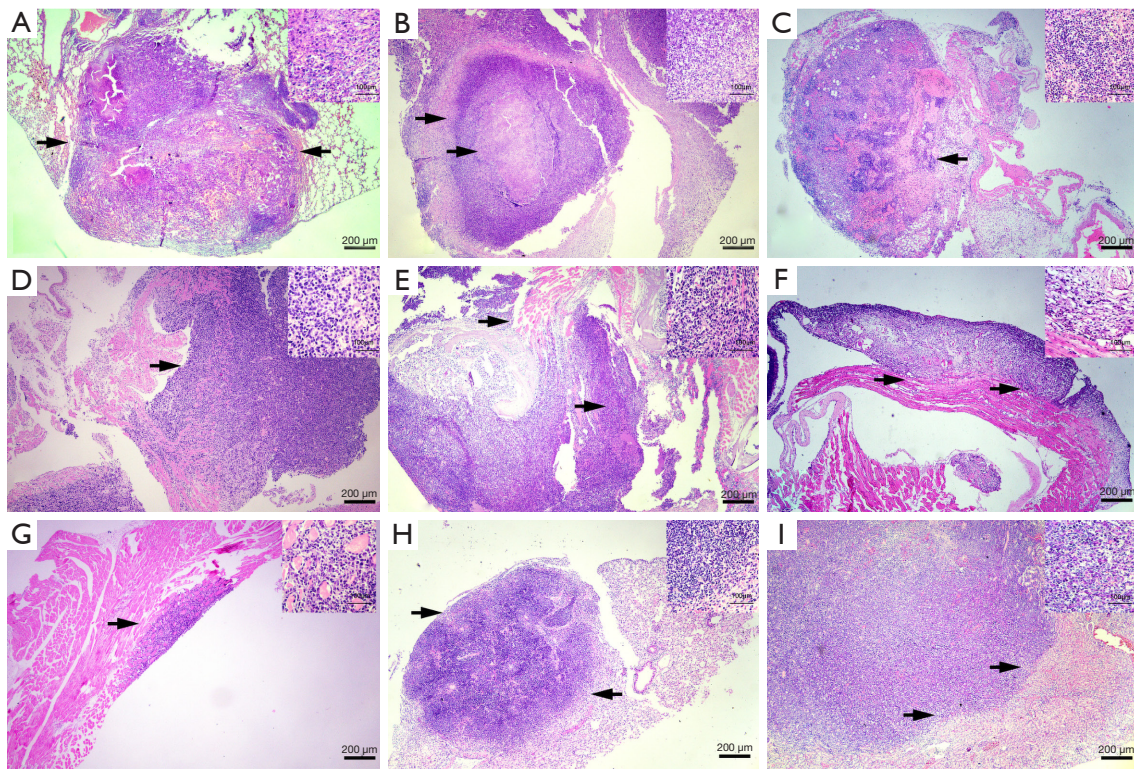
Figure 5 Pathology (H&E) of implanted tumor in the orthotopic models of lung cancer. (A,B) Solitary microscopic nodules surrounded by hemocytes, inflammatory cells, and normal lung tissue. With the tumor enlarged, necrosis and ulceration begin to appear inside. (C-F) Ipsilateral thoracic tissues infiltration, lymphomatous metastasis to the mediastinum, and thoracic spread to the diaphragm. (G,H) The tumor metastasized to the contralateral chest wall and right lung. (I) Renal metastasis was also found. The heterogeneity and morphological characteristics between primary tumor and metastasis were consistent (black arrows).

optimum tumor growth and development *in vivo* (22). An adequate and exceptional orthotopic model serves as the basis for both researches on the biology of lung cancer and the development of successful treatment regimens.

According to our knowledge, PDOX is a significant model used in translational research because it mimics the clinical pattern of metastasis (9). However, several of the drawbacks we discussed previously have limited its widespread adoption. Our study produced orthotopic lung cancer models by puncturing the lungs LLC tumor fragments. The primary innovation of this study compared to previously published orthotopic models is technique enhancement. First and foremost, tumor tissue fragments were used to create orthotopic models. The size of the tissue block is 1×1×1 mm, yet it contains sufficient malignant cells for tumor transplantation and maintains the heterogeneity of the tumor. In addition to malignant cells, the tumor microenvironment is composed of numerous cell types (stromal, endothelial, and immune

cells) and an extracellular matrix that works together to sustain the tumor. To research the causation and therapy of lung cancer, tumor fragments were employed to generate orthotopic models that can revert to the original condition of the tumor microenvironment and play a major role in the study of pathogenesis and treatment of lung cancer (23,24). In addition, tumor tissue fragments were implanted into the left lung, tumor development was localized and stabilized, the metastasis from the orthotopic site was more likely to occur, and the disease process may have been more precisely recapitulated (25,26). In particular, it achieved a minimally invasive impact comparable to cell suspension injection, and implantation techniques required no advanced surgical skills. Similarly, we chose the left lung as the receiver of the transplanted tumor since it had only 1 lobe. In addition to analyzing the appropriateness of the 8th or 9th intercostal as a puncture site, the angle and depth of the puncture, as well as any difficulties that arose, have been evaluated. In addition, BALB/c mice are affordable, simple to raise, and

2020

Gan et al. Establishment of the orthotopic model of lung cancer

have low dietary needs, making them ideal for use in most laboratories. Since the majority of immune function is preserved in these mice, these syngeneic mouse models may be utilized to examine the impact of immunotherapy on distant lung cancer metastases (27). Finally, getting clinical specimens of lung cancer is difficult. In addition, there are several benefits to utilizing LLC as a model, including increased tumorigenesis rates, a shorter time for tumor formation, and an appropriate supply of tumor tissue. All of these are essential for developing orthotopic models in practice.

The tumor pieces utilized to generate models were taken from a tumor cell line, which presented certain restrictions. Other than tumor cells, they contain few other components of the original tumor. We spent 2 months studying tumor growth and metastasis. The first time we discovered a tumor in the lung was 10 days after implantation, and during the entire observation period, just 1 distant metastasis was detected. Due to limited observation time, the exact moment of carcinogenesis was unknown, and many organic metastases disappeared. In addition, only 6 mice consented to the small-animal PET/CT scan, and no distant metastases were discovered because the scan was performed just once. Perhaps we could track systemic metastases by examining mice in batches weekly using dynamic scanning (28). Research funds were limited and some experiments cannot be carried out. In a forthcoming study, we will analyze these deficiencies further and create more rigorous tests to address them. In addition, we anticipate constructing orthotopic lung cancer models using tumor pieces derived from clinical patients.

Conclusions

This modified method was deemed reliable, reproducible, minimally invasive, simple, and straightforward. It might serve as the foundation for developing PDOXs of lung cancer.

Acknowledgments

Footnote

Reporting Checklist: The authors have completed the ARRIVE reporting checklist. Available at https://jtd.amegroups.com/article/view/10.21037/jtd-23-439/rc

Data Sharing Statement: Available at https://jtd.amegroups.com/article/view/10.21037/jtd-23-439/dss

Peer Review File: Available at https://jtd.amegroups.com/article/view/10.21037/jtd-23-439/prf

Conflicts of Interest: All authors have completed the ICMJE uniform disclosure form (available at https://jtd.amegroups.com/article/view/10.21037/jtd-23-439/coif). Yuan-Qiao He is an employee of Nanchang Royo Biotech Ltd. (Nanchang). The other authors have no conflicts of interest to declare.

Ethical Statement: The authors are accountable for all aspects of the work in ensuring that questions related to the accuracy or integrity of any part of the work are appropriately investigated and resolved. The Institutional Animal Care and Use Committee of Nanchang Royo Biotech Co., Ltd. approved all animal experiments (IACUC Issue No. RYE2020021801). Animal experiments were performed in Nanchang Royo Biotech Ltd. (Nanchang, China), in compliance with institutional guidelines for the care and use of animals.

References

1. Meuwissen R, Berns A. Mouse models for human lung cancer. Genes Dev 2005;19:643-64.
2. Gazdar AF, Hirsch FR, Minna JD. From Mice to Men and Back: An Assessment of Preclinical Model Systems for the Study of Lung Cancers. J Thorac Oncol 2016;11:287-99.
3. Bibby MC. Orthotopic models of cancer for preclinical drug evaluation: advantages and disadvantages. Eur J

Cancer 2004;40:852-7.

4. Madero-Visbal RA, Colon JF, Hernandez IC, et al. Bioluminescence imaging correlates with tumor progression in an orthotopic mouse model of lung cancer. Surg Oncol 2012;21:23-9.

5. Kim GT, Hahn KW, Yoon SY, et al. PLAG Exerts Anti-Metastatic Effects by Interfering with Neutrophil Elastase/PAR2/EGFR Signaling in A549 Lung Cancer Orthotopic Model. Cancers (Basel) 2020;12:560.

6. Liang TL, Li RZ, Mai CT, et al. A method establishment and comparison of in vivo lung cancer model development platforms for evaluation of tumour metabolism and pharmaceutical efficacy. Phytomedicine 2022;96:153831.

7. Nakajima T, Anayama T, Matsuda Y, et al. Orthotopic lung cancer murine model by nonoperative transbronchial approach. Ann Thorac Surg 2014;97:1771-5.

8. Hoffman RM. Metastatic orthotopic mouse models of lung cancer. Methods Mol Med 2003;74:457-64.

9. Hoffman RM. Patient-derived orthotopic xenografts: better mimic of metastasis than subcutaneous xenografts. Nat Rev Cancer 2015;15:451-2.

10. Wang X, Fu X, Kubota T, et al. A new patient-like metastatic model of human small-cell lung cancer constructed orthotopically with intact tissue via thoracotomy in nude mice. Anticancer Res 1992;12:1403-6.

11. Kang Y, Omura M, Suzuki A, et al. Proliferation of human lung cancer in an orthotopic transplantation mouse model. Exp Ther Med 2010;1:471-5.

12. Kawaguchi K, Han Q, Li S, et al. Efficacy of Recombinant Methioninase (rMETase) on Recalcitrant Cancer Patient-Derived Orthotopic Xenograft (PDOX) Mouse Models: A Review. Cells 2019;8:410.

13. Fujino H, Kondo K, Miyoshi T, et al. Establishment of patient-like SCID mouse model by orthotopically implanting primary cultured cells from surgically-resected lung cancer tissues. Oncol Rep 2003;10:1709-15.

14. Mordant P, Loriot Y, Lahon B, et al. Bioluminescent orthotopic mouse models of human localized non-small cell lung cancer: feasibility and identification of circulating tumour cells. PLoS One 2011;6:e26073.

15. He T, Huang Y, Zhang C, et al. Interleukin-17A-promoted MSC2 polarization related with new bone formation of ankylosing spondylitis. Oncotarget 2017;8:96993-7008.

16. Slaoui M, Fiette L. Histopathology procedures: from tissue sampling to histopathological evaluation. Methods Mol Biol 2011;691:69-82.

17. Fidler IJ. The pathogenesis of cancer metastasis: the

'seed and soil' hypothesis revisited. Nat Rev Cancer 2003;3:453-8.

18. Paget S. The distribution of secondary growths in cancer of the breast. 1889. Cancer Metastasis Rev 1989;8:98-101.

19. Jarry U, Bostoën M, Pineau R, et al. Orthotopic model of lung cancer: isolation of bone micro-metastases after tumor escape from Osimertinib treatment. BMC Cancer 2021;21:530.

20. Pu X, Zhang R, Wang L, et al. Patient-derived tumor immune microenvironments in patient-derived xenografts of lung cancer. J Transl Med 2018;16:328.

21. Hirsch FR, Scagliotti GV, Mulshine JL, et al. Lung cancer: current therapies and new targeted treatments. Lancet 2017;389:299-311.

22. Koga Y, Ochiai A. Systematic Review of Patient-Derived Xenograft Models for Preclinical Studies of Anti-Cancer Drugs in Solid Tumors. Cells 2019;8:418.

23. Altorki NK, Markowitz GJ, Gao D, et al. The lung microenvironment: an important regulator of tumour growth and metastasis. Nat Rev Cancer 2019;19:9-31.

24. Taromi S, Kayser G, von Elverfeldt D, et al. An orthotopic mouse model of small cell lung cancer reflects the clinical course in patients. Clin Exp Metastasis 2016;33:651-60.

25. Hoffman RM. Orthotopic metastatic (MetaMouse) models for discovery and development of novel chemotherapy. Methods Mol Med 2005;111:297-322.

26. Johnston MR, Mullen JB, Pagura ME, et al. Validation of an orthotopic model of human lung cancer with regional and systemic metastases. Ann Thorac Surg 2001;71:1120-5.

27. Saito R, Kobayashi T, Kashima S, et al. Faithful preclinical mouse models for better translation to bedside in the field of immuno-oncology. Int J Clin Oncol 2020;25:831-41.

28. Otani T, Otsuka H, Kondo K, et al. Utility of respiratory-gated small-animal PET/CT in the chronologic evaluation of an orthotopic lung cancer transplantation mouse model. Radiol Phys Technol 2015;8:266-77.

(English Language Editor: J. Jones)